To be published in Optics Letters:

Title: Rapid ellipsometric imaging characterization of nanocomposite films with an artificial neural network.

Authors: PATRICK KFOURY,Yann Battie,Aotmane En Naciri,Michel Voue,Nouari Chaoui

Accepted: 08 January 24

Posted 08 January 24

DOI: https://doi.org/10.1364/OL.514616

© 2024 Optica

OPTICA
PUBLISHING GROUP
Formerly OSA

Rapid ellipsometric imaging characterization of nanocomposite films with an artificial neural network.

PATRICK KFOURY,[1] YANN BATTIE,[1,*] AOTMANE EN NACIRI,[1] MICHEL VOUE,[2] NOUARI CHAOUI[1]

[1] LCP-A2MC, Université de Lorraine, ICPM, 1 Bd Arago 57070 Metz, France
[2] LPMO, Université de Mons, Institut de Recherche en Science et Ingénierie des Matériaux, Place du Parc, 20, 7000 Mons, Belgium
*yann.battie@univ-lorraine.fr

Received XX Month XXXX; revised XX Month, XXXX; accepted XX Month XXXX; posted XX Month XXXX (Doc. ID XXXXX); published XX Month XXXX

Imaging ellipsometry is an optical characterization tool that is widely used to investigate the spatial variations of the opto-geometrical properties of thin films. As ellipsometry is an indirect method, ellipsometric map analysis requires a modeling step. Classical methods such as the Levenberg–Marquardt algorithm (LM) are generally too time-consuming to be applied on a large data set. In this way, an artificial neural network (ANN) approach was introduced for the analysis of ellipsometric map. As a proof of concept this method was applied for the characterization of silver nanoparticles embedded in poly-(vinyl alcohol) film. We demonstrate that the LM and ANN gives similar results. However, the time requires for the ellipsometric map analysis decreases from 15 days for the LM to 1s for the ANN. This suggests that ANN is a powerful tool for fast spectroscopic ellipsometric imaging analysis.

OPTICA PUBLISHING GROUP
Formerly OSA

Spectroscopic ellipsometry (SE) is one of the most powerful techniques for investigating the opto-geometrical properties of materials. SE is based on the measurement of the change of polarization state of light reflected from sample. This technique, was previously used to determine the complex refractive index of materials, the optical anisotropy, the stoichiometry of alloys, the thickness and the roughness of thin films [1-5], the profile of diffraction grating [6-8] or the volume fraction and shape distribution of nanoparticles (NP) contained in nanocomposite films [9-10]. The beam size of standard ellipsometer which limits the lateral resolution, is about few millimeters. However, the trends of devices miniaturization require the development of ellipsometric set up with microscopic scaled resolution. Cohn *et al.* have addressed this issue by introducing an imaging ellipsometer [11]. This kind of set-up allows recording the spatial variation of ellipsometric spectra with a lateral resolution as small as 1 µm. This technique was previously used to investigate the homogeneity and the optical properties of 2D nanomaterials [12-13], optical waveguides [14], patterned biosensors [15], diffraction gratings [16] or plasmonic materials [17]. Two images representing the ellipsometric angles Ψ and Δ are recorded for each wavelength. As SE is an indirect characterization tool, the extraction of physical parameters of the sample from the recorded spectra requires a modeling step. However, the analysis of this huge data cube remains challenging. To reduce the data size, pixels can be gathered into region of interest (ROI) by using the binning process. However, this approach assumes that opto-geometrical properties are homogeneous inside a ROI. On the other end, the fitting of the full ellipsometric map by using classical optimization algorithm such the Levenberg-Marquard algorithm (LM) is often time consuming. Even the interpolation of the Ψ and Δ values limits to power of the analysis to 1-parameter optical models. Recent works have suggested that ellipsometric spectra, recorded without spatial resolution, can be exploited by using an artificial neural network (ANN) [4,6-8,18-23]. Fried *et al.* have used an ANN analysis of ellipsometric spectra to determine the damage profile induced by ion implantation in silicon-on-insulator structure [18]. This neural analysis procedure was also used to analyze ellipsometric map [19]. They also modified the sample selection strategy to improve the convergence of the learning algorithm toward global minima [20]. Urban III *et al.* have implemented a cascade of several ANN to improve the accuracy of the ANN analysis [21]. Recently, some authors. have shown that ANN could be a fast, accurate, and useful approach to exploit ellipsometric measurements performed on Ge-Sb-Te alloys [22] or perovskite materials [23]. In our previous work, we have also demonstrated that ANN is less sensitive to local minima and solves the inverse problem in a shorter time than the LM algorithm [24]. Despite these development in ellipsometric characterization, this approach has never been used to exploit ellipsometric images. Indeed, it was only applied to punctual ellipsometric measurements or ellipsometric map with a small number of pixels [4, 19].

In this context, the aim of this letter is to demonstrate the feasibility of the complete analysis of ellipsometric images by using a neural network. Compare to punctual ellipsometric measurements or standard ellipsometric map, these images are composed of a large number of pixels. The fine analysis of this kinds of images generally constitutes a challenge. For this proof of concept, spectroscopic imaging ellipsometry measurements were performed on thin poly-(vinyl alcohol) (PVA) film containing silver nanoparticles (NPs) and deposited on silicon wafer. This sample was elaborated according to the Porel method [25]. Briefly, a (0.12g/ml) aqueous solution of PVA (MW: 13000 – 23000) is first prepared and stirred vigorously at 90°C for 1 hour, and at room temperature for 23h. Then, silver nitrate ($AgNO_3$) is added to the solution in order to obtain an $AgNO_3$ concentration of 0.0475 g/ml. After that, the solution was deposited by spin coating at 5000 rpm on a silicon substrate. Finally, the central part of the obtained sample was irradiated with a 150W Xenon lamp for 2h at an irradiance value of 2000 W/m^2. Twenty maps of ellipsometric angles Ψ and Δ were recorded at 10 wavelengths in the 380–812 nm spectral range by means of an EP3-SE spectroscopic nulling imaging ellipsometer (Accurion GmbH). This corresponds to a data-cube of 8424600 elements. The objective was a Nikon 10X (NA=0.21). The angle of incidence was set to 60°. The spatial resolution was estimated to 0.52x0.52 µm^2 per pixel, without binning of the images. Ellipsometric spectra are also recorded by using a classical ellipsometer (UVISEL, Horiba), without spatial resolution. The measurements are performed at an angle of incidence of 70° in the 270nm-900nm spectral range and a spot size of about 800 µm.

As ellipsometry is an indirect technique, each spectrum must be analyzed with a model which reflects the physical properties of the sample. In our case, the model consists in Ag NPs embedded in a PVA film on a silicon substrate. As previously shown [9-10], the effective dielectric function (ε_{eff}) of the film can be described by using the shape distributed effective medium theory (SDEMT):

$$\varepsilon_{eff} = \frac{(1-f)\varepsilon_m + f\beta\varepsilon_{NP}}{1-f+f\beta}. \quad (1)$$

f is the volume fraction of Ag NPs. ε_m and ε_{NP} are the dielectric function of PVA matrix and silver, respectively. The coefficient β is given by:

$$\beta = \frac{\varepsilon_m}{3}\iint P(L_1,L_2)\sum_{i=1}^{3}\frac{1}{\varepsilon_m + L_i(\varepsilon_{NP}-\varepsilon_m)}dL_1 dL_2. \quad (2)$$

$P(L_1,L_2)$ is the normalized distribution of the depolarization factors L_i of NP which is directly related to the distribution of NP shape. These parameters must respect the following sum rule:

$$\sum_{i=1}^{3} L_i = 1. \quad (3)$$

In the following, we assume that the distribution $P(L_1,L_2)$ is described by a Gaussian distribution centred on the locus of spherical NP:

$$P(L_1,L_2) = Ce^{-\frac{(L_1-\frac{1}{3})^2+(L_2-\frac{1}{3})^2}{2\sigma^2}}. \quad (4)$$

σ and C are the standard deviation and the normalization factor of the distribution, respectively. Three parameters must be determined for each pixel positions: f, σ and the film thickness h. The spatial variations of f, σ and h deduced from ellipsometric measurements by using the LM algorithm are depicted in Figure 1 a-c. These maps highlight the inhomogeneities of nanocomposite film at the microscale. This spatial inhomogeneities are probably related to the NPs growth mechanism and especially the diffusion and aggregation of NPs in the film. Some statistical parameters can be extracted from ellipsometric maps. The mean value of f, h and σ are 4.75%, 253 nm and 0.099, respectively. These results are close to the f, h and σ values of 4.14%, 253 nm and 0.99 by using a classical ellipsometer, without spatial resolution. The standard deviation of f, h and σ are 0.72%, 15 nm and 0.017, respectively. The root mean square error between the measured and modeled spectra is estimated to 0.013 ± 0.019. This value is in the same order of magnitude as the accuracy of the ellipsometer confirming the validity of the model.

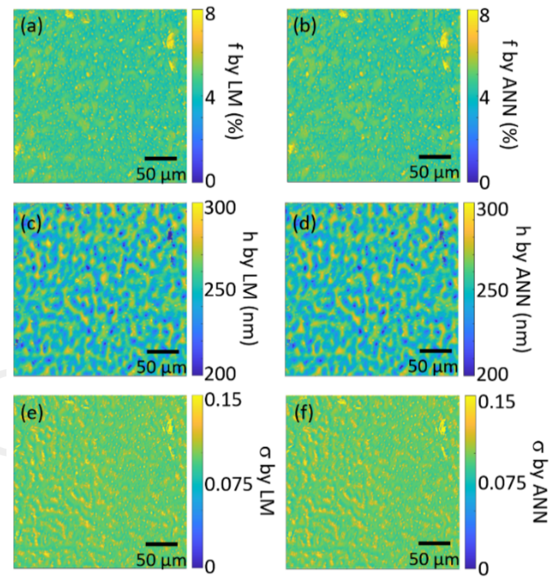

Figure 1: Specially-resolved parameters of the optical model : (a)(b) Ag NP volume fraction ; (c)(d) Film thickness ; (e) and (f) Width of the normal distribution of the depolarization factors. (a)(c)(e) images: are obtained from a LM inversion. (b)(d)(f) images are obtained from ANN.

Despite local information on the sample can be deduced from imaging ellipsometry, the analysis of the ellipsometric maps with the LM algorithm requires 15 days computing time. Thus, this procedure is too time consuming to be used for routine characterizations. Other optimization algorithm should be found to overcome this issue. Since ANN is a universal and parsimonious approximator [26], it can be considered as a promising candidate to solve these kinds of problem with a shorter computing time. As a proof of concept, we implement in Matlab multilayer perceptron (Figure 2(a)) composed of a single hidden layer and an output layer of neurons. The calculations are performed with a multi-core personal computer (Intel Core i7 7700k, 4 cores, 3.6 GHz). The layers are linked together by weighted synaptic connections. Each neuron m applies a specific transfer function g to its weighted inputs:

$$o_m = g\left(\sum_{p=0}^{N} w_{m,p}x_p\right). \quad (5)$$

OPTICA PUBLISHING GROUP Formerly OSA

$w_{m,p}$ is the weight of the synapse which links the input x_p and the neuron m. The transfer functions of the hidden neurons and output neurons are sigmoid and linear functions, respectively. The input vector consists in the ellipsometric parameters Is and Ic. The number of hidden neurons is arbitrary set to 30. The output layer is composed of 3 neurons. The outputs of the ANN are f, σ and h. The relationship between the input and output of the ANN is learned during the training step. This step requires a large number of input/output data. 400000 samples are randomly generated from a uniform distribution by taking the parameters f, σ and h in the following ranges.

$$0.8\% \leq f \leq 30\%,$$
$$100\,nm \leq h \leq 400\,nm,$$
$$0.0007 \leq \sigma \leq 0.3.$$

The generation of these data takes almost 6h. Then, the ellipsometric spectra of these samples were simulated by using our model. These couples of input/output data were then split into three corpuses: the training data (280000 couples), the validation data (80000 couples), and the test data (40000 couples). The ANN was then trained with the training data by using the back propagation Levenberg–Marquardt algorithm [27]. During the training step, the synaptic weights were adjusted to minimize the error between the training data and the ANN output. To avoid the overfitting, the training was stopped by using the early stopping technique, i.e. until the error evaluated from the validation data increases. The training of the ANN takes almost 3h. Once trained, the ANN can be reused to analyze several ellipsometric images without any further training step. The performances of the ANN were evaluated on the test data. Figure 2(b)(c)(d) shows the value of f, σ and h determined by the ANN as a function of the corresponding value of the test data. Linear variation is found between the f, σ and h values predicted by the ANN and the nominal ones. The slope and intercept value are close to 1 and 0, respectively. The root mean square error on f, σ and h are estimated to 0.1%, 2 nm and 0.003, respectively. These results obtained on test data, confirm the high level of operating performance of the ANN. Nevertheless, this performance was evaluated on virtual samples.

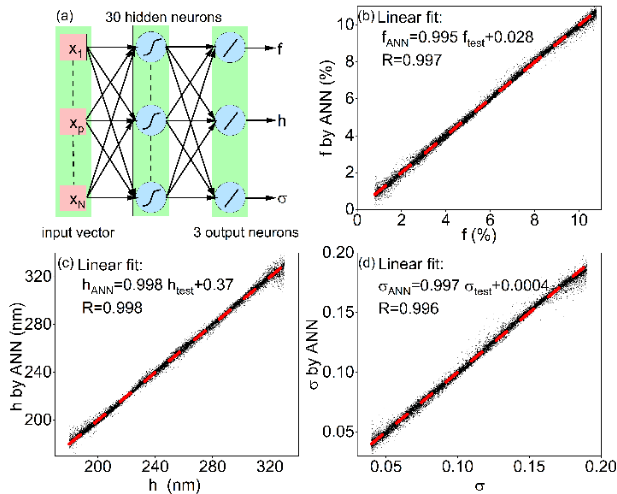

Figure 2: (a) Schematic representation of the ANN used in this work. Comparison between the (b) f, (c) h, and (d) σ values estimated by the ANN and the theoretical values of the test data. The linear regressions are represented by the red dashed line.

It is therefore important to evaluate the performance of our ANN on an experimental ellipsometric map. Figure 1(d)(e)(f) shows the f, σ and h maps deduced from the analysis of the ellipsometric map with the ANN. These maps are similar to those obtained by the LM algorithm. To give a more quantitative comparison, the results determined by the ANN for each pixel are against those deduced from the ANN (Figure 3). Each point of Figure 3 is located along the identity line. The root mean square error between the f, h and σ, as estimated by ANN and LM are 0.3%, 4.8 nm and 0.008, respectively. In addition, both methods give similar f, h and σ distributions. Thus, it can be concluded that the ANN globally reproduces the results obtained by the LM. The mean value of the root mean square error between the measured and the modeled spectra from the ANN is estimated to 0.014 ± 0.024. This value is close to that obtained by the LM, suggesting that the LM and ANN have the same accuracy. We can also remark that for 9 pixels, the LM falls into a local minimum located at $\sigma = 0.3$. However, the ANN gives other solutions with a smaller root mean square error for these pixels. It probably converges toward the global minima. Indeed, as shown by several works ANN is more robust than LM to local minima [21, 24].

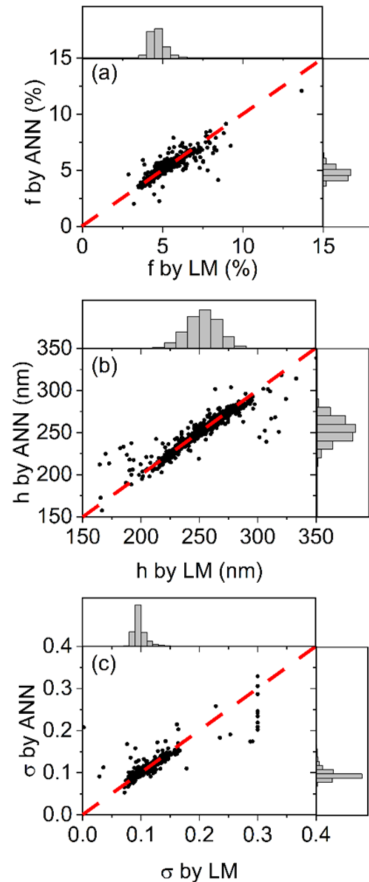

OPTICA
PUBLISHING GROUP
Formerly OSA

Figure 3: Comparison between the (a) f, (b) h, and (c) σ values and histogram estimated by the ANN and LM. Each dot represents 1 pixel of the ellipsometric map. The red dashed line represents the identity line.

In summary, a new method based on an ANN is introduced to analyze spectroscopic ellipsometric maps. This method, applied to silver NPs in PVA film, allows investigating the spatial variation of film thickness, volume fraction and the shape distribution of NPs. This neural and LM data processing gives similar results with the same accuracy. However, the computing time required for the analysis of the 842460 spectra of Ψ and Δ which composed the ellipsometric map decreases from 15 days for the LM to 1s for the ANN. This can be considered as real drastic improvement for in-line SE imaging characterization. In addition, once trained, the ANN can be reused without any further training step. As also reported by several works [21, 24], ANN is less sensitive to local minima of the error function than LM. Finally, the ANN ellipsometric map processing is fairly flexible and can be easily applied to other kind of samples., although requiring a specific training for each class of sample.

Funding. This work was supported by the PHC Tournesol Program (46237UL).

Disclosure. Authors declare no conflict of interest.

Authors' contributions. These authors contributed equally to the work

Availability of data and material. The datasets generated during and/or analysed during the current study are available from the corresponding author on reasonable request.

OPTICA PUBLISHING GROUP Formerly OSA

References

1. W. Zhou, Y. Liu, Y. Yin, W. Ma, and Z. Huang, Z., "Investigation on the optical properties of annealed Mn-Co-Ni-O thin films by spectroscopic ellipsometry," Opt. Lett. **44,** 2701 (2019).
2. G. Jayaswal, Z. Dai, X. Zhang, M. Bagnarol, A. Martucci, and M. Merano, "Measurement of the surface susceptibility and the surface conductivity of atomically thin MoS_2 by spectroscopic ellipsometry," Opt. Lett. **43,** 703 (2018).
3. D. Schmidt, B. Booso, T. Hofmann, E. Schubert, A. Sarangan, and M. Schubert, "Generalized ellipsometry for monoclinic absorbing materials: determination of optical constants of Cr columnar thin films," Opt. lett. **34,** 992 (2009).
4. Y. Battie, A. C. Valero, D. Horwat, and A. E. Naciri, "Rapid ellipsometric determination and mapping of alloy stoichiometry with a neural network," Opt. Lett. **47,** 2117 (2022).
5. P. Petrik, L. P Biró, M. Fried, T. Lohner, R. Berger, C. Schneider, J. Gyulai, and H. Ryssel, "Comparative study of surface roughness measured on polysilicon using spectroscopic ellipsometry and atomic force microscopy," Thin Solid Films **315,** 186 (1998)
6. I. Gereige, S. Robert, S. Thiria, F. Badran, G. Granet, and J. J. Rousseau, "Recognition of diffraction-grating profile using a neural network classifier in optical scatterometry," J. Opt. Soc. Am. A **25,** 1661 (2008).
7. M. G. Tchéré, S. Robert, Z. S. Fawzi, B. Bayard, D. Jamon, and C. Gourgon, "Experimental identification of a grating profile using neural network classifiers in optical scatterometry," Appl. Opt. **60,** 7929 (2021).
8. T. Novikova, A. De Martino, P. Bulkin, Q. Nguyen, B. Drévillon, V. Popov, and A. Chumakov, "Metrology of replicated diffractive optics with Mueller polarimetry in conical diffraction," Opt. Express, **15,** 2033 (2007).
9. Y. Battie, A. En Naciri, N. Chaoui, Y. Le Gall, D. Muller, M. Carrada, and D. Mathiot, "Plasmonic properties of implanted Ag nanoparticles in SiO2 thin layer by spectroscopic ellipsometry," J. Appl. Phys. **122,** 085308 (2017)
10. Y. Battie, I. Izquierdo-Lorenzo, A. Resano-Garcia, A. En Naciri, S. Akil, P. M. Adam, and S. Jradi, "Determination of gold nanoparticle shape from absorption spectroscopy and ellipsometry," Appl. Surf. Sci. **421,** 301 (2017).
11. R. F. Cohn, J. W. Wagner, and J. Kruger, "Dynamic imaging microellipsometry: theory, system design, and feasibility demonstration," Appl. Opt. **27,** 4664 (1988).
12. S. Funke, B. Miller, E. Parzinger, P. Thiesen, A. W. Holleitner, and U. Wurstbauer, "Imaging spectroscopic ellipsometry of MoS_2," J. Phys. Condens. Matter, **28,** 385301 (2016).
13. A. Matković, A. Beltaos, M. Milićević, U. Ralević, B. Vasić, D. Jovanović, and R. Gajić, "Spectroscopic imaging ellipsometry and Fano resonance modeling of graphene," J. Appl. Phys. **112,** 123523 (2012).
14. P. Moreno-Zarate, A. Gonzalez, S. Funke, A. Días, B. Sotillo, J. del Hoyo, M. Garcia-Pardo, R. Serna, P. Fernandez, and J. Solis, "Imaging ellipsometry determination of the refractive index contrast and dispersion of channel waveguides inscribed by fs-laser induced ion-migration," Phys. Status Solidi A **215,** 1800258 (2018).
15. C. Qi, X. S. Tian, S. Chen, J. H. Yan, Z. Cao, K. G. Tian, G. F. Gao, and G. Jin, "Detection of avian influenza virus subtype H5 using a biosensor based on imaging ellipsometry," Biosens. Bioelectron. **25,** 1530 (2010).
16. S. Liu, W. Du, X. Chen, H. Jiang, and C. Zhang, « Mueller matrix imaging ellipsometry for nanostructure metrology," Opt. Express **23,** 17316 (2015).
17. C. Guyot, P. Leclère, and M. Voué, "Gold nanoparticles growing in a polymer matrix: What can we learn from spectroscopic imaging ellipsometry?," J. Vac. Sci. Technol. B **38,** (2020).
18. M. Fried, and P. Masa, "Backpropagation (neural) networks for fast pre-evaluation of spectroscopic ellipsometric measurements," J. Appl. Phys. **75,** 2194-2201 (1994).
19. M. Fried and, L. Rédei, "Non-destructive optical depth pro®ling and real-time evaluation of spectroscopic data," Thin Solid Films **364,** 64-74 (2000).
20. L. Rédei, M. Fried, I. Bársony, and H. Wallinga, "A modified learning strategy for neural networks to support spectroscopic ellipsometric data evaluation," Thin Solid Films **313,** 149-155 (1998).
21. F. K. Urban III, D. Barton, and N. I. Boudani, "Extremely fast ellipsometry solutions using cascaded neural networks alone," Thin Solid Films **332,** 50-55 (1998).
22. Y. Li, Y. Wu, H. Yu, I. Takeuchi, and R. Jaramillo, "Deep learning for rapid analysis of spectroscopic ellipsometry data," Adv. Photonics Res. **2,** 2100147 (2021).
23. S. M. Kim, S. D. H. Naqvi, M. G. Kang, H.-e Song, and S. Ahn, "Optical characterization and prediction with neural network modeling of various stoichiometries of perovskite materials using a hyperregression method," Nanomaterials **12,** 932 (2022).
24. Y. Battie, S. Robert, I. Gereige, D. Jamon, and M. Stchakovsky, "Demonstration of the feasibility of a complete ellipsometric characterization method based on an artificial neural network," Appl. Opt. **48,** 5318-5323 (2009).
25. S. Porel, N. Venkatram, D. Narayana Rao, and T.P Radhakrishnan, "In situ synthesis of metal nanoparticles in polymer matrix and their optical limiting applications," J. Nanosc. Nanotechnol. **7,** 1887 (2007).
26. G. Cybenko, "Approximation by superpositions of a sigmoidal function," Mathematics of control, signals and systems **2,** 303 (1989).
27. R. Rojas, Neural networks: a systematic introduction (Springer Science & Business Media, Springer, Berlin, 2013).

OPTICA
PUBLISHING GROUP
Formerly OSA